First observation of Hα redshifted emission in RR Lyr

D. Gillet, B. Mauclaire, T. Garrel, T. Lemoult, Ph. Mathias, T. de France, J.-S. Devaux, H. Boussier, D. Verilhac, G. Brabant, et al.

A&A 607, A51 (2017)
DOI: 10.1051/0004-6361/201629897

Astronomy & Astrophysics

First observation of Hα redshifted emission in RR Lyr*

Evidence of a supersonic infalling motion of the atmosphere

D. Gillet[1], B. Mauclaire[2], T. Garrel[3], T. Lemoult[4], Ph. Mathias[5], T. de France[6], J.-S. Devaux[7], H. Boussier[8], D. Verilhac[9], G. Brabant[10], J. Desbordes[11], O. Garde[12], and the GRRR Collaboration[13,⋆⋆]

[1] Observatoire de Haute-Provence – CNRS/PYTHEAS/Université d'Aix-Marseille, 04870 Saint-Michel l'Observatoire, France
e-mail: denis.gillet@osupytheas.fr
[2] Observatoire du Val de l'Arc, route de Peynier, 13530 Trets, France
e-mail: bma.ova@gmail.com
[3] Observatoire de Fontcaude, 19 Av. du Hameau du golf, 34990 Juvignac, France
[4] Observatoire de Chelles, 23 Av. Hénin, 77500 Chelles, France
[5] Observatoire Midi-Pyrénées, IRAP, Université de Toulouse, CNRS, UPS, CNES, Tarbes, 31400 Toulouse, France
[6] Observatoire de Mèze, 5 Imp. des Tourterelles, 34140 Mèze, France
[7] Observatoire OAV, 13 rue du Moulin, 34290 Alignan-du-Vent, France
[8] 115 Av. du général de Gaulle, 84450 Saint-Saturnin-les-Avignon, France
[9] Les Trucs, 26420 Saint-Agnan en Vercors, France
[10] 42 chemin de la Beaume, 26190 Saint-Laurent-en-Royans, France
[11] 5 rue Edmond Gondinet, 75013 Paris, France
[12] Observatoire de la Tourbière, 45 chemin du Lac, 38690 Chabons, France
[13] Observatoire de Haute-Provence, 04870 Saint-Michel l'Observatoire, France

Received 14 October 2016 / Accepted 22 August 2017

ABSTRACT

Context. The so-called Hα third emission occurs around pulsation phase $\varphi = 0.30$. It has been observed for the first time in 2011 in some RR Lyrae stars. The emission intensity is very weak, and its profile is a tiny persistent hump in the red side-line profile.
Aims. We report the first observation of the Hα third emission in RR Lyr itself (HD 182989), the brightest RR Lyrae star in the sky.
Methods. New spectra were collected in 2013−2014 with the AURELIE spectrograph (resolving power $R = 22\,700$, T152, Observatoire de Haute-Provence, France) and in 2016−2017 with the eShel spectrograph ($R = 11\,000$, T035, Observatoire de Chelles, France). In addition, observations obtained in 1997 with the ELODIE spectrograph ($R = 42\,000$, T193, Observatoire de Haute-Provence, France) were reanalyzed.
Results. The Hα third emission is clearly detected in the pulsation phase interval $\varphi = 0.188-0.407$, that is, during about 20% of the period. Its maximum flux with respect to the continuum is about 13%. The presence of this third emission and its strength both seem to depend only marginally on the Blazhko phase. The physical origin of the emission is probably due to the infalling motion of the highest atmospheric layers, which compresses and heats the gas that is located immediately above the rising shock wave. The infalling velocity of the hot compressed region is supersonic, almost 50 km s^{-1}, while the shock velocity may be much lower in these pulsation phases.
Conclusions. When the Hα third emission appears, the shock is certainly no longer radiative because its intensity is not sufficient to produce a blueshifted emission component within the Hα profile. At phase $\varphi = 0.40$, the shock wave is certainly close to its complete dissipation in the atmosphere.

Key words. stars: variables: RR Lyrae – stars: atmospheres – shock waves

1. Introduction

The variability of RR Lyr, the brightest RR Lyrae star in the sky, has been discovered by the Scottish astronomer Williamina Fleming at Harvard (Pickering et al. 1901). The light curve exhibits a period of about 0.5667 days (13.6 h) that is attributed to pulsation. It also presents amplitude and phase modulations with a period of about 39 days, the so-called well-known Blazhko effect (Blažko 1907). Its physical origin still remains a mystery, although several interesting hypotheses have recently been proposed to explain the Blazhko phenomenon (Smolec 2016; Kovács 2016). In addition, the pulsation and Blazhko periods change slightly during their respective cycles, and the ephemerides therefore have to be updated regularly (e.g., Le Borgne et al. 2014).

Preston et al. (1965) reported the first detailed spectroscopic study of RR Lyr during a whole Blazhko cycle, but this investigation was limited to the rising part of the pulsation light curve. During this phase, Preston et al. (1965) observed line doubling in metallic lines as well as emission in the Hα profile.

⋆ Based in part on observations made at the Observatoire de Haute-Provence (CNRS), France.
⋆⋆ The Groupe de Recherche sur RR Lyrae (GRRR) is an association of professionals and amateur astronomers leading high-resolution spectroscopic and photometric monitoring of complex phenomena such as the RR Lyrae Blazhko effect.

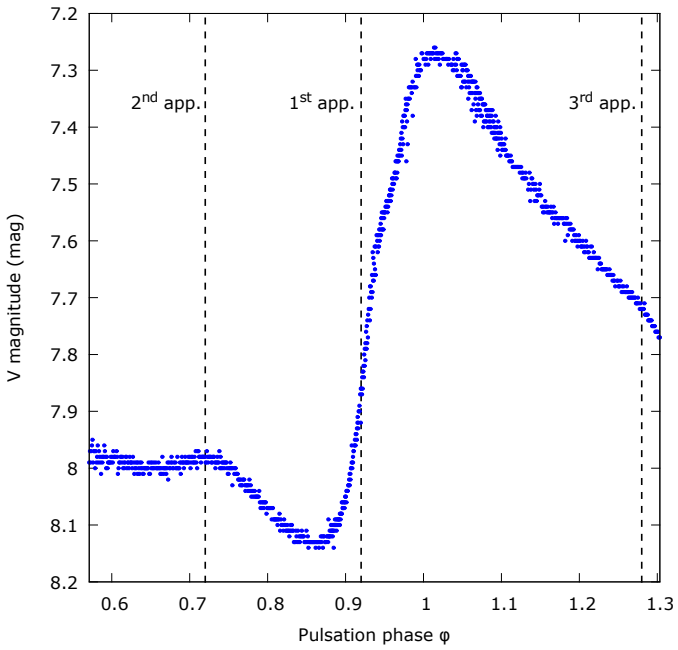

Fig. 1. RR Lyr light curve covering the pulsation cycle from $\varphi = 0.57$ to $\varphi = 1.31$. V magnitudes were measured with the G filter (490−580 nm) corresponding to the V photometric Johnson-Cousins bandwidth (490−590 nm) on a Schmidt-Cassegrain 5″ telescope. Observations were made between June 10 and 15, 2013, when the Blazhko phase was in the interval $\psi = 0.74-0.87$. Dashed lines show the phases around which the three different emissions appear within the Hα profile.

These phenomena were interpreted by means of a shock wave propagation, following the work of Schwarzschild (1952), who showed that a shock wave can produce these particular profiles in population II Cepheids. Preston et al. (1965) also showed that during its outward propagation, the shock increases in intensity and velocity. In addition, during the Blazhko cycle, the critical zone in the stellar atmosphere where the wave breaks moves up and down. These observational results were modeled by Fokin & Gillet (1997), who computed more than 20 nonlinear nonadiabatic pulsation models. Although the code they used is purely radiative, convection is thought to affect the results only weakly since the helium ionization zone is located deeper in the envelope (Xiong et al. 1998). In particular, Fokin & Gillet (1997) showed that five main shocks occur during a pulsation cycle.

In this paper, the pulsation phase is noted φ, and $\varphi = 0.0$ corresponds to the maximum luminosity. The Blazhko phase is noted ψ and has its maximum at $\psi = 0.0$, the time of the highest luminosity amplitude observed during a Blazhko cycle.

During a pulsation cycle in RR Lyrae stars, as we show in Fig. 1, there are three successive appearances of hydrogen emissions. Preston (2011) classified these "apparitions" according to the date of the discovery of the emission line. Hereafter, we keep the name apparition proposed by Preston (2011) since the second and third emissions are not always observed at each pulsation cycle and consequently are like "ghost emissions".

The first apparition is a strong blueshifted Hα emission in RR Lyrae stars that was first reported by Struve & Blaauw (1948). Because it was the first such detection, Preston (2011) called this strongest Hα emission "first apparition". It occurs immediately before the luminosity maximum, around pulsation phase $\varphi = 0.92$, and may be caused by the sum of five shocks that are theoretically expected according to Fokin & Gillet (1997); the strongest of these shocks is initiated by the κ-mechanism. The first self-consistent theory was proposed by Fadeyev & Gillet (2004). The model considers a stationary shock wave within an homogeneous medium consisting solely of atomic hydrogen with the five first bound levels and the continuum, allowing a computation of the hydrogen emission line profiles. Their most remarkable result is that the velocity inferred from Doppler shifts of the Balmer emission lines is roughly one-third of the shock wave velocity, with a mean value of about 130 km s^{-1}, depending on the pulsation cycle.

The second apparition was discovered by Gillet & Crowe (1988) as a small blueshifted emission component within the large Hα absorption profile in two stars: X Ari (a non-Blazhko RR Lyrae star), and RR Lyr itself. This small emission appears during the bump, that is, before the luminosity minimum near the pulsation phase $\varphi = 0.72$. The bump was interpreted by Hill (1972) as the consequence of a shock or collision between atmospheric layers. Gillet & Crowe (1988) attributed this "second apparition" to a secondary shock that is produced when the outer atmospheric layers, following a ballistic motion, impact inner layers. For RR Lyr, this secondary emission seems absent at the Blazhko minimum phase ($\psi = 0.50$), but it is observable immediately before the Blazhko maximum ($\psi = 0.97$). This means that an amplitude threshold may exist to induce this secondary shock.

The third apparition was recently found in some RR Lyrae stars Preston (2011), but not in RR Lyr itself. This weak and redshifted emission shoulder appears within the Hα absorption near the pulsation phase $\varphi = 0.30$, after maximum light, and occurs in Blazhko and non-Blazhko stars. It has never been detected before in RR Lyr. Preston (2011) did not explain its physical origin, but Chadid & Preston (2013) suggested that this emission component might be caused by a weakly supersonic and infalling shock wave at the beginning of atmospheric compression. However, it should be noted that these authors did not explain how such a compression shock alone can produce redshifted emission. In contrast to the explanation by Chadid & Preston (2013), Gillet & Fokin (2014) proposed that the redshifted emission component of Hα might be produced by the main shock. This weak emission should be observed when the main shock propagates far enough from the photosphere, that is, when the shock intensity is very high. In this case, the emission profile would become a P Cygni type profile, and would be the consequence of the large extension of the expanding atmosphere.

In this paper, we present for the first time the observation of the third Hα emission in RR Lyr itself. In Sect. 2 we describe observational and data reduction processes. The detection of the hydrogen line third apparition is presented in Sect. 3, while its physical origin is discussed in Sect. 4. Finally, some concluding remarks are given in Sect. 5.

2. Observations and data analysis

2.1. Data acquisition

Since we are especially interested in the Hα third emission that occurs in the pulsation phase interval $0.2 \lesssim \varphi \lesssim 0.4$, we reexamined previous published spectra and obtained new detections of the third emission at this particular step of the pulsation and for various Blazhko phases. We finally used data obtained from spectrographs between 1997 and 2017.

– ELODIE spectrograph: attached to the 193 cm telescope at the Observatoire de Haute-Provence, it is described

Table 1. Characteristics of the RR Lyr spectra.

Night (yyyy-mm-dd)	JD (-2 400 000)	Tel.	Obs.	Spectro.	Resolving power	RE (pixel)	$\lambda_{start} - \lambda_{end}$ (Å)	T_{exp} (min)	S/N	N	φ_{start}	φ_{end}	ψ
1997-08-09	50 670	193	OHP	ELODIE	42 000	2.1	3800–6 800	8	70	1	0.311	0.321	0.61
1997-08-30	50 691	193	OHP	ELODIE	42 000	2.1	3800–6800	5	98	4	0.277	0.301	0.14
2013-09-04	56 540	152	OHP	AURELIE	22 700	2.8	6500–6700	10	80	16	0.074	0.289	0.95
2014-09-14	56 915	152	OHP	AURELIE	22 700	2.8	6500–6700	10	90	12	0.332	0.471	0.86
2016-12-03	57 726	35	CHELLES	eShel	11 000	3.2	4300–7100	30	114	2	0.207	0.281	0.54
2017-03-26	57 838	35	CHELLES	eShel	11 000	3.2	4300–7100	30	98	1	0.227	0.264	0.44
2017-03-29	57 842	35	CHELLES	eShel	11 000	3.2	4300–7100	10	52	2	0.231	0.256	0.54
2017-04-02	57 846	35	CHELLES	eShel	11 000	3.2	4300–7100	10	70	4	0.255	0.304	0.64

in Baranne et al. (1996). Observations were performed in 1996–1997 in the context of a survey led by D. Gillet and published in Chadid et al. (1999). We used some spectra from these observations to verify the third emission during different Blazhko phases. Typical exposure times were between 5–8 min, leading to a signal-to-noise ratio (S/N) of about 50 per pixel for a resolving power of $R = 42\,000$. It appears that this relatively low S/N is not enough for a suitable detection of the third emission, and we are left with only two Blazkho phases. In addition, for the night of 1997-08-30, four spectra were stacked to improve the S/N per pixel to 80. This echelle spectrograph allows observing the whole visible domain (3900–6800 Å), but it suffers from overlapping in blue orders that prevents us from observing some important lines such as the Na I doublet or the Balmer H_β line.

– AURELIE spectrograph: attached to the 152 cm telescope at the Observatoire de Haute-Provence, it is described in Gillet et al. (1994). Data used in this paper were collected during two separate nights in September 2013 (16 spectra) and September 2014 (12 spectra). High-resolution spectra ($R = 22\,700$) were obtained with a typical exposure time of 10 min, leading to a mean S/N of about 85 per pixel. The spectral domain is relatively short: 6500–6700 Å.
– eShel spectrograph: attached to an automated 35 cm telescope at the Observatoire de Chelles (France), the fiber-fed eShel spectrograph was described in Thizy & Cochard (2011) and was built by Shelyak Instruments[1]. A few spectra were gathered from December 2016 to April 2017 to search for the third emission at other Blazhko phases. The exposure times varied between 10 and 30 min (less than 4% of the pulsation period), providing an S/N per pixel of between 50 and 100 for a resolving power of $R = 11\,000$. The spectral domain is spread over 4300–7100 Å. The detector used for the eShel spectrograph is an Atik 460EX CCD (Sony ICX694 sensor).

Observations are summarized in Table 1, where the columns provide the date of the night, the corresponding Julian Date, the telescope (Tel.) and observatory (Obs.), the attached spectrograph (Spectro.), its resolving power, its resolution element RE, the spectral domain, the typical exposure time T_{exp} used for the night, the mean S/N per pixel in the λ6630 region, the number N of spectra considered, and finally the start and end of the pulsation phase and the Blazhko phase for each night.

2.2. Data reduction

All observations were reduced using classical operations such as preprocessing (bias and dark subtraction, flat-fielding, masking of bad pixels, spectrum extraction, wavelength calibration, correction for instrumental response), and the observations provide spectra in the heliocentric rest frame. For ELODIE spectra, the online pipeline was used as described in Chadid & Gillet (1996). The AURELIE and eShel observations were reduced using subpackages of the the Audela[2] software, SpcAudace[3] and a dedicated echelle package, respectively, that were originally implemented.

Then we normalized the spectra to the local continuum in the Hα region, and a Savitsky-Golay filter (Savitzky & Golay 1964) was applied for visual detection to remove noise while preserving the spectral resolution of each data set. Nevertheless, all measures were made on unfiltered spectra.

Wavelengths were further corrected for the heliocentric velocity and radial velocity of RR Lyr, which is also called the γ-velocity, using $RV = -73.5$ km s^{-1} (Chadid & Gillet 1996). Our Hα line profile observations show that the absorption line center is not centered on the laboratory wavelength (represented as a vertical line in Figs. 2–8), unlike the line profiles presented in Preston (2011), which seem to present anomalous wavelength corrections.

Finally, Figs. 2–9 represent the spectra in the detector histogram mode. Depending on the spectrograph, the resolution element is between 2.1 and 6.0 pixels (see Table 1). Thus, the resolving power is directly visible in the spectra.

2.3. Ephemerides computation

Periods and phases both change for the pulsation and also for the Blazhko variations. Since we are interested in peculiar phases, it is fundamental to use a current and adapted ephemeris. Recently, Le Borgne et al. (2014) showed that the pulsation period alternates between two primary pulsation states, defined as pulsation over a "long" (0.56684 d) and a "short" (0.56682 d) period, with intervals of 13–16 yr. A direct consequence is that the ephemeris used by Chadid et al. (1999) for the ELODIE observations (1997) is not relevant since it concerns the epoch 1982–1989. We therefore preferably used ephemerides provided by Le Borgne et al. (2014) for the ELODIE and AURELIE observations. For the more recent 2016–2017 data, an epoch out of that for the ephemeris provided by Le Borgne et al. (2014), the pulsation period P_P was computed using the difference between two O–C minima from the GEOS RR Lyr web database[4] and close to our 2016–2017 observations. The reference HJD maximum light ($HJD0_P$) was also provided by this database. A

[1] http://www.shelyak.com

[2] http://www.audela.org
[3] http://spcaudace.free.fr
[4] http://rr-lyr.irap.omp.eu

Table 2. Ephemerides used to compute the pulsation and Blazhko phase.

Epoch	Pulsation		Blazhko	
	$HJD0_P$ (−2 400 000)	Period P_P (d)	$HJD0_B$ (−2 400 000)	Period P_B (d)
1997	50 456.7090[a]	0.5668174[b]	49 631.312[c]	39.06[b]
2013	56 539.3428[a]	0.5667975[b]	56 464.481[d]	39.0[b]
2014	56 914.5507[a]	0.56684[b]	56 881.627[d]	39.0[b]
2017	57 861.6319[a]	0.566793[a]	57 354.322[d]	39.0[b]

Notes. Maximum light HJD and periods are from [(a)] GEOS; [(b)] Le Borgne et al. (2014); [(c)] Chadid et al. (1999); [(d)] this paper.

summary of the ephemerides for the different data sets is provided in Table 2.

It is more difficult to determine the Blazhko phase because the Blazhko period P_B does not follow the variation of the pulsation period, but presents rather erratic changes (Le Borgne et al. 2014). Moreover, during 2014, the photometric O−C were historically low (close to nil), preventing an easy computing of the Blazhko period. Therefore, in order to determine the maximum light amplitude dates $HJD0_B$, we developed an innovative method based on equivalent width and main shock velocities based on our three years of spectral observations, which will be described in a forthcoming paper (Gillet et al., in prep.). We expect an uncertainty of ±2 days on $HJD0_B$ and of ±0.2 day on P_B. The ephemerides were computed with the period P_B = 39.0 d (Le Borgne et al. 2014). However, for the 1997 observations, the maximum light amplitude date was taken from Chadid et al. (1999) and the Blazhko period is given by Le Borgne et al. (2014), that is, $P_{B\,1997}$ = 39.06 d. Blazhko ephemerides used for the different data sets is summarised in Table 2 too.

3. Observation of the hydrogen third emission in RR Lyr

3.1. Evidence of the third emission

Figures 2 (2013-09-04) and 3 (2014-09-14) show the evolution of the Hα line profile during the phase intervals φ = 0.074−0.289 and φ = 0.332−0.471, respectively.

No appreciable structure appears in the blue wing of the Hα absorption profile, while the red wing is clearly affected by a weak hump for the relevant phase intervals φ = 0.188−0.289 and φ = 0.332−0.407. This hump represents the so-called Hα third emission. We note that the deeper analysis was conducted on the 2013 and 2014 observations, since their temporal sampling is best suited for the follow-up of the third emission. We emphasize that all the considered observations of Table 1 also present this third emission, regardless of the phase ψ of the Blazhko cycle.

3.2. Extraction of the third emission

To highlight the third emission within the Hα profile, which manifests itself as a hump in the spectra, we chose to subtract the different absorption profiles in this spectral region. Since the atmospheric dynamics may strongly affect the stellar line profile, we did not use a synthetic stellar spectrum since these latter are computed for a static atmosphere. The different shock waves occurring in the atmosphere during the pulsation cycle (five main shock waves for RR Lyr, see Fokin & Gillet 1997) induce high velocity gradients and a strong rise (by up to two or three times) in the level of turbulence.

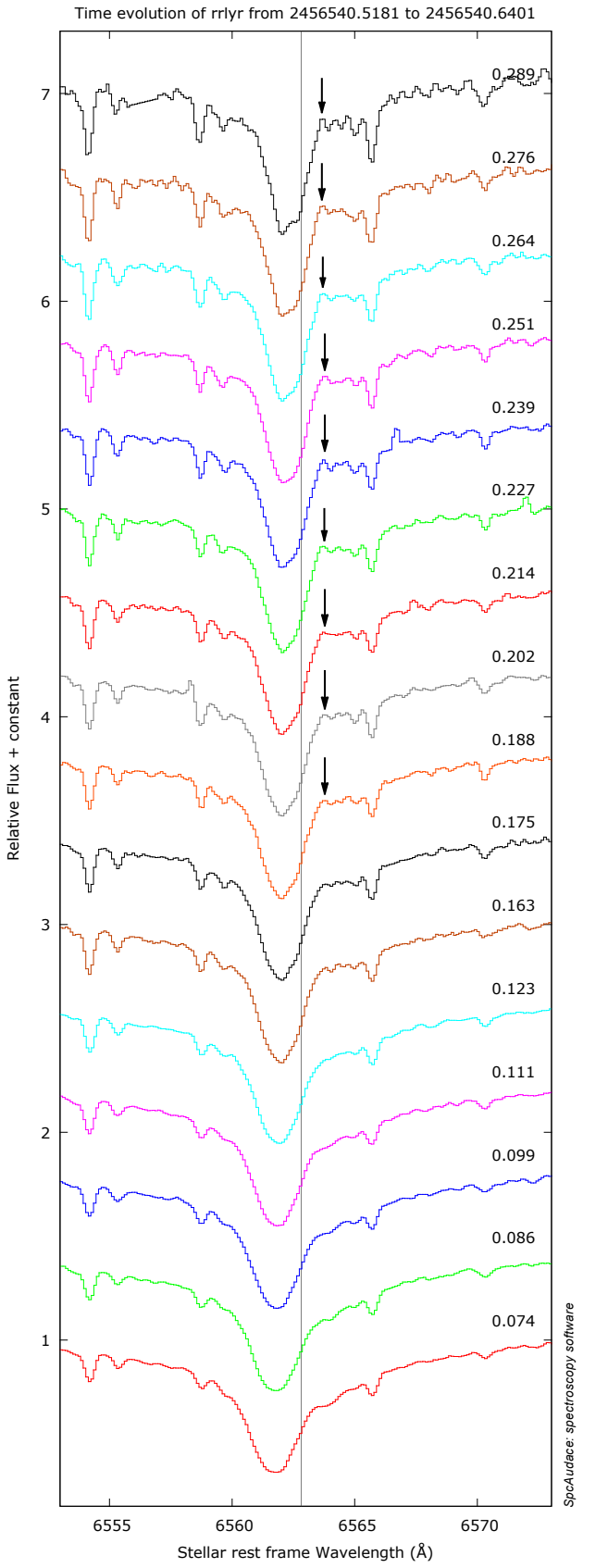

Fig. 2. Evolution of the Hα line profile of RR Lyr for the night 2013-09-04 (Blazhko phase ψ = 0.95). The third emission is the weak hump indicated by the arrows, and it occurs for φ = 0.188−0.289. Weak absorption features are telluric lines. The vertical line indicates the Hα line laboratory wavelength in the stellar rest frame.

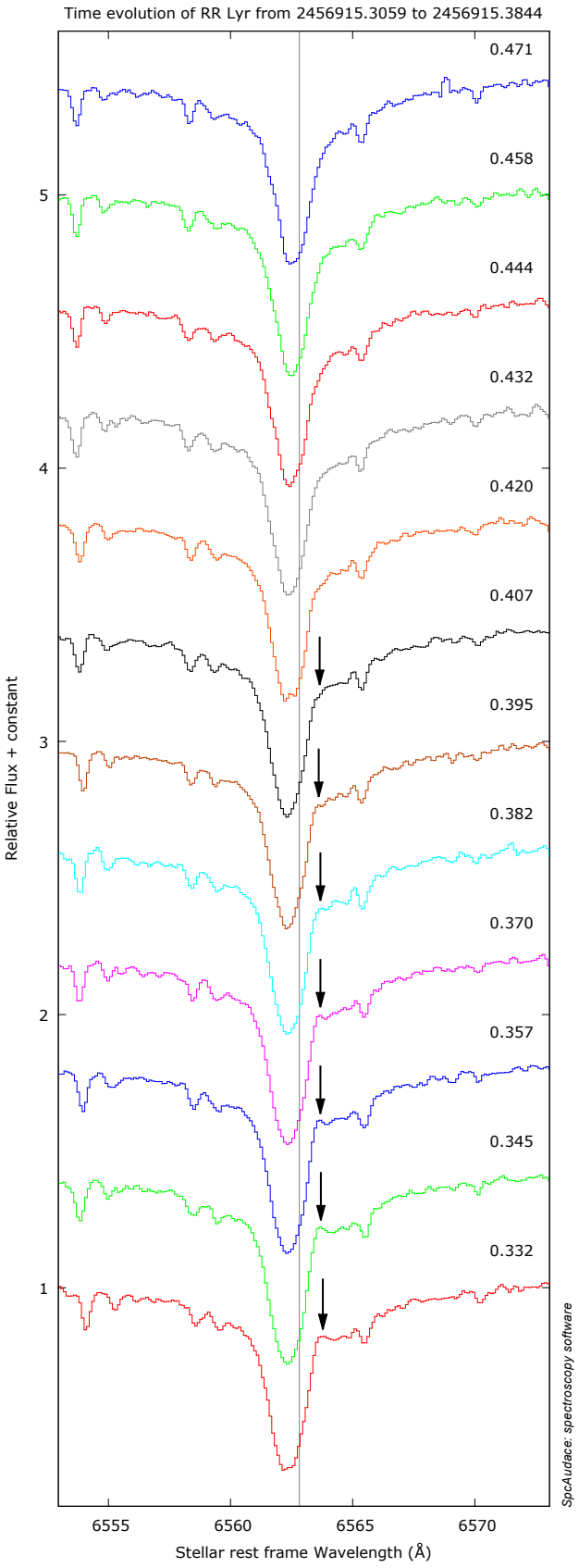

Fig. 3. Evolution of the Hα line profile of RR Lyr for the night 2014-09-14 (Blazhko phase $\psi = 0.86$). The third emission is the weak hump indicated by the arrows, and it occurs for $\varphi = 0.332-0.407$. The weak absorption features are telluric lines. The vertical line indicates the Hα line laboratory wavelength in the stellar rest frame.

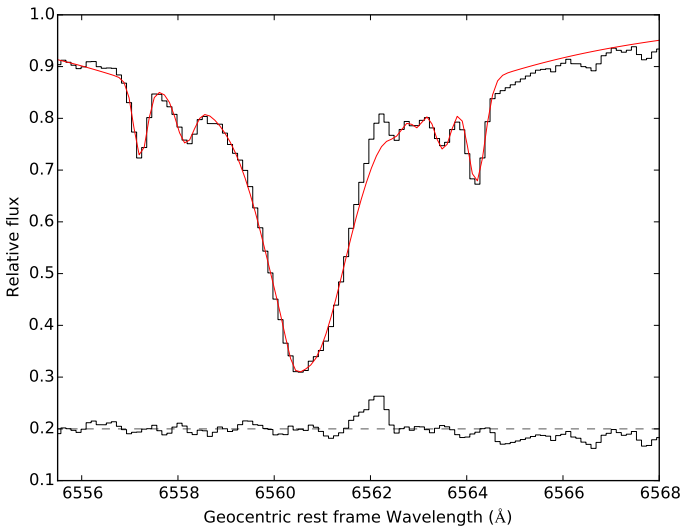

Fig. 4. Observed Hα spectral domain (black) and its resulting fit (red) for the Hα absorption profile and seven telluric lines computed for the 2013-09-04 night at $\varphi = 0.239$. The difference is plotted at the bottom of the figure with a +0.2 vertical offset for clarity. The residual clearly shows the third emission component within the red wing of the Hα absorption profile.

We used individual (Gaussian) profiles instead, regardless of their origin, stellar or telluric, using the PySpecKit library (Ginsburg & Mirocha 2011). This Python package uses as input the number of lines present in the spectral domain considered together with their wavelengths, which are fixed, and it provides the residual flux and widths for each component. The Hα absorption profile, which presents Stark wings, was modeled using three Gaussians of different widths. Other features have a telluric origin (λ = 6557.21, 6558.12, 6560.43, 6562.68, 6562.82, 6563.56, and 6564.26 Å). We note that the computations were made in the geocentric rest frame to match the telluric lines, and then we transformed back to the stellar rest frame. We emphasize that no known lines (whether stellar or of telluric origin) are present at the third emission expected wavelength.

An example of the resulting fit is provided in Fig. 4 together with the residual obtained by subtracting the fit from the initial profile: the third emission around 6562 Å (geocentric rest frame) is now clearly visible. This procedure was carried out for all the spectra used in this paper, and examples of residuals at different phases are presented in Figs. 5 and 6.

3.3. Spectral characteristics of the third emission

Hence, the fitting process allows a direct study of the third emission profile, and some characteristics of the line can be derived, such as the associated velocity (hereafter V_{e3}), the full width at half-maximum (FWHM), the residual flux (RF), and the equivalent width (EW), as a function of the pulsation phase. For the two AURELIE nights, these quantities are represented in Fig. 7. The typical uncertainties are about 2 km s^{-1} for the velocity data, 0.5% for the flux, and 80 mÅ and 8 mÅ for the FWHM and EW quantities, respectively. The RF peaks at about 10% above the continuum, at a level similar to other measurements in other RR Lyrae stars. While the RF and EW show a continuous variation between the two epochs, the FWHM instead shows a constant value for the 2013 data and a decreasing behavior during 2014.

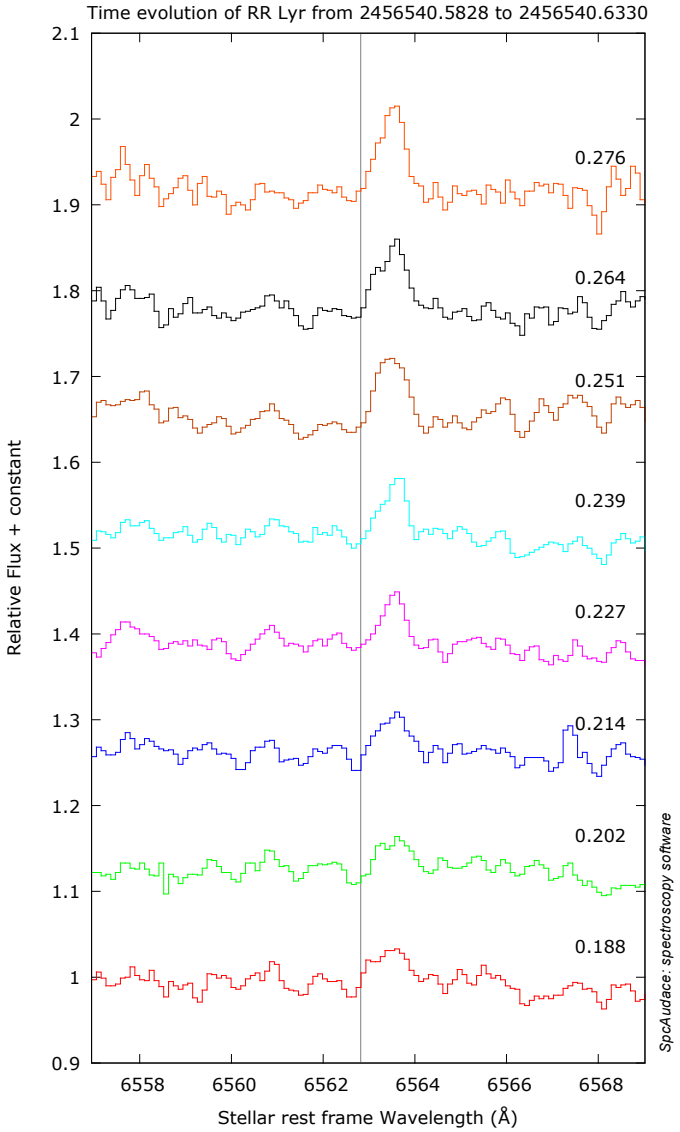

Fig. 5. Evolution of the residuals for the night 2013-09-04 for pulsation phases $\varphi = 0.188-0.276$. The vertical line indicates the Hα line laboratory wavelength in the stellar rest frame.

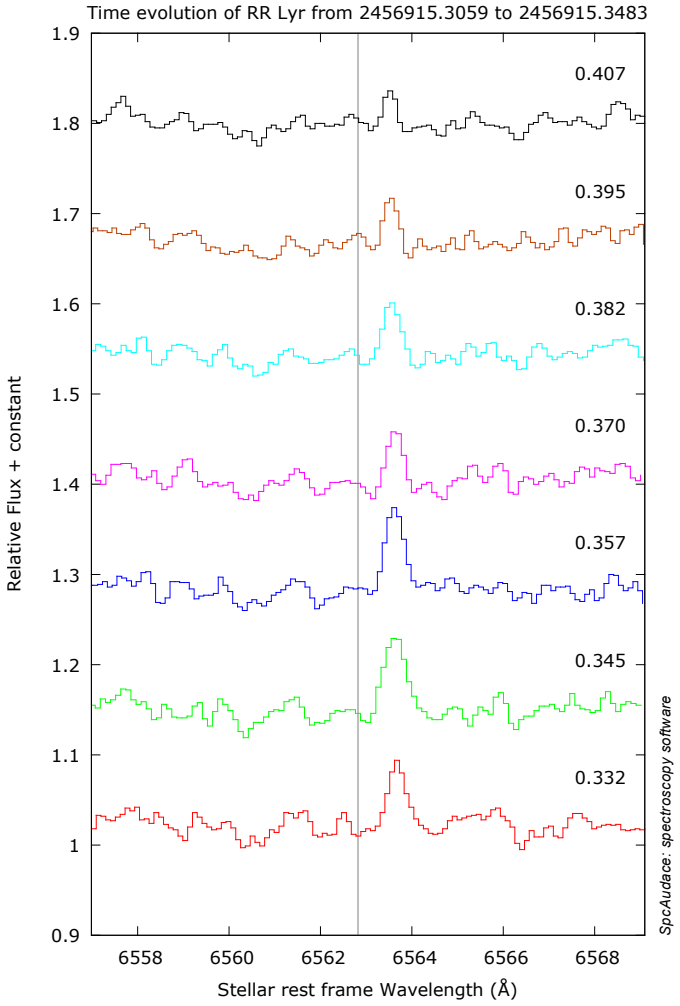

Fig. 6. Evolution of the residuals for the night 2014-09-14 for pulsation phases $\varphi = 0.332-0.407$. The vertical line indicates the Hα line laboratory wavelength in the stellar rest frame.

For the two nights, the velocity seems to follow a regular slow-down at a rate of about 200 cm s^{-2} for the 2014 data and about 100 cm s^{-2} for the 2013 data, which shows that a breaking mechanism is active. The difference between the slope associated with each night might be due either to a different atmospheric dynamics or to a different Blazhko phase, since the nights are separated by about 10% of the Blazhko period.

The variation in the FWHM and EW suggests that temperature effects are maximum at about $\varphi \sim 0.3$, and they may be linked to the inward ballistic motion.

3.4. Evolution of the third emission

Since the atmospheric dynamics seems to change between the 2013 and 2014 observations, it is interesting to extend the study of these spectral characteristics to other Blazhko phases. Figure 8 presents spectra obtained over the 20 years of observations presented in Table 1. It is clear that the third apparition is observed at all Blazhko phases. While the flux of the third emission varies by up to 10% during the pulsation phase, there is no such a difference with the Blazhko phase: the third emission seems not larger during the two Blazhko maxima observed in 2013 and 2014 ($\psi = 0.95$) than during the Blazhko minima of 2016 and 2017 ($\psi = 0.54$).

To summarize, the third emission is present for about 20% of the pulsation period, from $\varphi = 0.188-0.407$, with a typical flux of about 10% of the continuum. This emission is clearly redshifted, by about 35 km s^{-1} in the stellar rest frame. Finally, its characteristics seems to be independent of the Blazhko phase.

4. Physical origin of the hydrogen third emission

4.1. Still-active infalling motion

According to the observations reported in this paper, the third hydrogen emission first appears near the pulsation phase $\varphi = 0.188$ (Fig. 2) and is observed until $\varphi = 0.407$ (Fig. 3). At this stage, photospheric layers should rise within the atmosphere since the shock wave passage starts at $\varphi = 0.92$. However, the upper atmosphere may still follow an infall ballistic motion. Only observable in the eShel observations because of the poor order overlapping in the ELODIE data, the Na I line profile doubles during night 2017-03-26 ($\varphi \sim 0.227$, $\psi = 0.44$, Fig. 9), which is representative of the other eShel spectra as well.

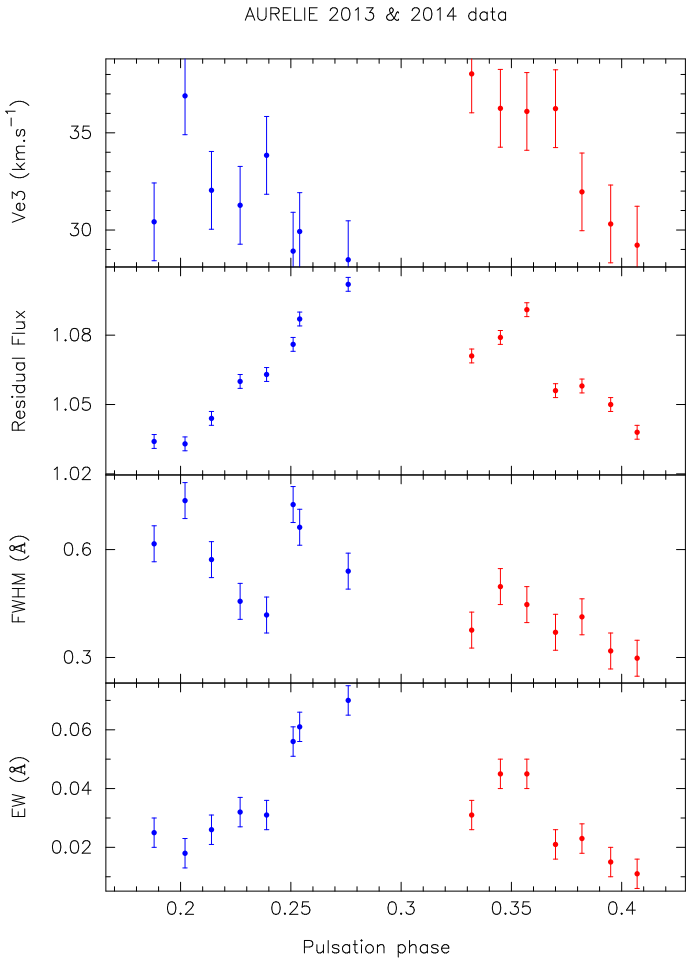

Fig. 7. Third-emission line characteristics for the nights 2013-09-04 (blue) and 2014-09-14 (red). *From top to bottom* we show the Doppler velocity in the stellar frame, the RF, the FWHM, and the EW.

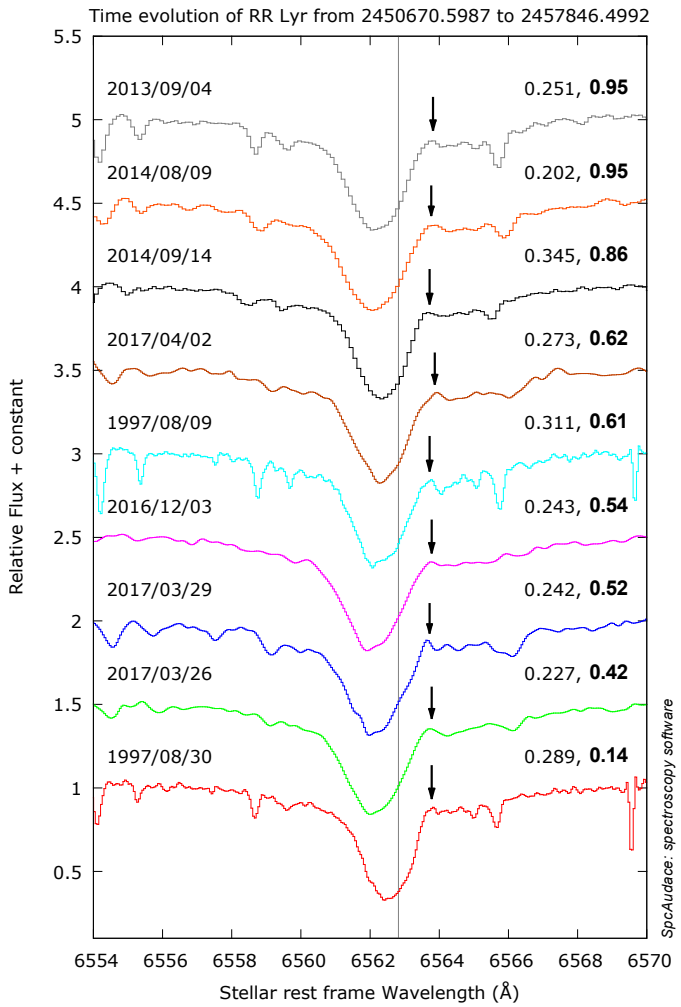

Fig. 8. Hα profile of RR Lyr for the 1997 to 2017 observations. Pulsation and Blazhko (in bold) phases (*right*) and observation dates (*left*) are indicated. The third emission is present at all Blazhko phases despite the different spectral resolutions and S/N. The detector pixel is shown in each spectrum. The vertical line shows the Hα line laboratory wavelength in the stellar rest frame.

While the blue component is related to the outward shock wave passage, the red component refers to the material falling back on the star. Therefore, at $\varphi \sim 0.227$, there is still a free-fall motion of the upper atmosphere. Unfortunately, since only one spectrum (which in addition has $T_{\rm exp} = 30$ min) has been obtained in that night, it is not possible to follow the evolution of the two components. Thus, we can infer from this observation that during the third-emission phase, the shock wave is located between the two Na I layers, and it is related to the line doubling phenomenon.

4.2. Supersonic infalling motion

The redshifted velocity of the Hα third emission gives an idea of the compression rate in the atmosphere. For the 2013 observations with pulsation phases $\varphi = 0.188-0.276$, the velocity of the redshifted emission remains approximately constant with a value of about 31 km s^{-1}, while for the 2014 observations with pulsation phases $\varphi = 0.332-0.407$, the velocity continuously decreases from 39 km s^{-1} to 32 km s^{-1} (Fig. 7) around an average value of 35 km s^{-1}. If the pulsation cycles are different, it seems clear that the velocity of the redshifted emission component maintains an approximately similar average value with pulsation phase. Thus, the atmospheric compression rate does not vary much in the phase interval $\varphi = 0.188-0.276$, while it seems to slowly increase in the interval $\varphi = 0.332-0.407$. There would therefore be a first phase during which the compression ratio would remain stable before starting to slowly decrease.

In 2014, the intensity of the emission reached a maximum near the pulsation phase $\varphi \sim 0.350$ (see Fig. 6), which must correspond to the strongest atmospheric heating. In 2013, the strongest emission intensity must certainly occur after $\varphi = 0.276$, but unfortunately, we do not have observations after this phase. On the other hand, in 2013, the third emission appears to be wider than in 2014. This would indicate that the temperature, and therefore the compression rate, would be higher during this pulsation cycle. However, it is clear that new observations of good quality are necessary to confirm this type of variation from one pulsation cycle to another.

The two sodium absorption components are separated by about 60 km s^{-1}, corresponding to the velocity difference between the two layers in opposite motion. The upward velocity of the gas is maximum immediately behind the shock front. However, because of the strong gravity of RR Lyr ($g_\star \sim 250$ cm s^{-2} at the RR Lyr photospheric radius, see Fossati et al. 2014), this velocity decreases continuously when moving away from the shock front, in the wake. Because the red component is shifted by about 50 km s^{-1} with respect to the sodium laboratory wavelength in

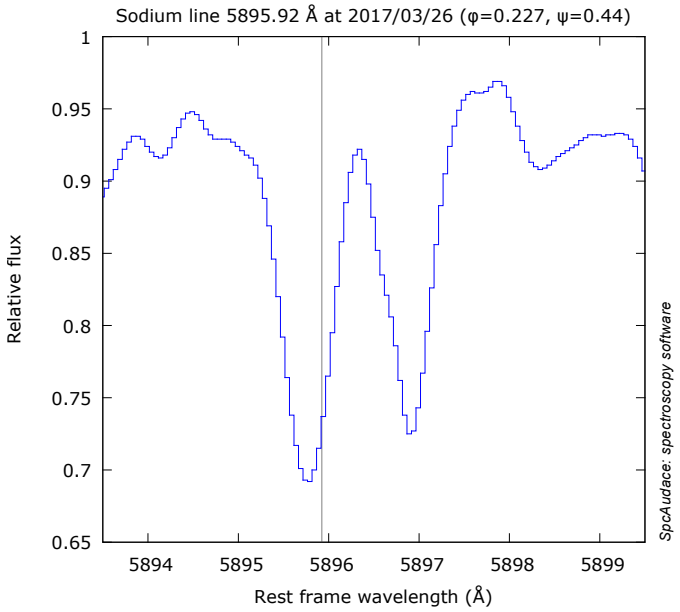

Fig. 9. Na I λ5895.92 (D1) profiles of RR Lyr for $\varphi = 0.227$ on the night of 2017-03-26. The Blazhko phase is $\psi = 0.44$, that is, close to the minimum. The vertical line indicates the sodium line laboratory wavelength in the stellar rest frame. Note that two strong telluric lines are blanketing the center of the D2 component, which is different to the D1 component (Hobbs 1978).

the stellar rest frame, this means that the infalling motion of the highest part of the atmosphere is largely supersonic (Mach number around 5 for a sound speed near 10 km s^{-1}). Consequently, the shock propagates in a higher-density medium compared to a static atmosphere with a classical decreasing density law. Future observations of the evolution of the Na I blue component velocity should test this assumption of a deceleration with the pulsation phase.

4.3. Shock front velocity

No direct observations are available, such as a blue component emission on the spectra during the phase interval $\varphi = 0.188-0.407$, that could help to directly measure the shock wave velocity.

According to Gillet & Fokin (2014), the shock front velocity varies from 130 km s^{-1} at $\varphi = 0.902$ to 115 km s^{-1} at $\varphi = 0.927$. These values are based on the shock models developed by Fadeyev & Gillet (2004), who derived

$$V_{\rm shock} \cong 3c\frac{(\lambda_{\rm e1} - \lambda_0)}{\lambda_0}, \quad (1)$$

where $\lambda_{\rm e1}$ is the wavelength of the maximum intensity of the Hα first-apparition emission and λ_0 its laboratory wavelength. On the other hand, because the D3 helium near the pulsation phase $\varphi = 1.04$ is a P Cygni profile, it implies that the shock velocity corresponds to the expansion rate of the gas shell, which is about 60 km s^{-1} (Gillet & Fokin 2014). Thus, the shock strongly decelerates between the pulsation phases 0.902 and 1.04. Since in the phase interval $\varphi = 0.188-0.407$ the shock does not produce any emission component within the Hα profile (see below), we can reasonably estimate that the shock intensity is weak and that the velocity of the front is much lower than 60 km s^{-1}.

Moreover, since the blue component of the sodium line is weakly blueshifted (−10 km s^{-1}), while the red component is strongly redshifted (50 km s^{-1}), it can even be considered that the shock may have a velocity lower than that of the infalling gas. Ultimately, in the phase interval $\varphi = 0.188-0.407$, the shock wave is no longer radiative, hence no emission component appears. It may even be close to its complete dissipation in the upper atmosphere. A stellar shell of a thickness of a few hundred kilometers and a radius on the order of 1.35 times the photospherical radius is probably dynamically unstable if its velocity is not sufficiently high (supersonic).

4.4. Weakening of the radiative shock shell

When the intensity of the main shock wave is strong enough, a significant extension of the atmosphere, and a consecutive P Cygni profile, are possible. This was clearly observed at $\varphi = 1.04$ with the D3 helium line (Gillet et al. 2016). Since it is reasonable to assume a continuation of the propagation of the shock shell at least until $\varphi = 1.04$, Gillet & Fokin (2014) suggested that the third Hα emission component is also a P Cygni profile. This explanation is plausible even though the emission is not centered on the laboratory wavelength in the stellar rest frame. As shown by Wagenblast et al. (1983), an advancing shell can produce a redshifted emission depending on the spectral line formation parameters such as the local line width, the geometrical extension of the emitting layer, the optical thickness, and especially the velocity gradient.

However, our recent observation on 2017-03-26 (see Fig. 9) of the sodium line doubling at $\varphi \sim 0.227$ shows that the infalling motion of the upper layers of the atmosphere compresses the low layers that are located immediately above the photosphere. The plasma created by this intense compression is most likely the cause of the third Hα emission component. Moreover, the shock wave velocity is lower than 60 km s^{-1}, as discussed above. Consequently, the explanation by Wagenblast et al. (1983) is not necessary or is not valid here to justify the third emission because the shock velocity is probably too weak to induce pertinent parameters for a redshifted third emission.

4.5. Atmospheric structure near $\varphi = 0.3$

At the phase $\varphi \sim 0.3$, the deepest photospheric layers are close to their maximum radius (Fokin & Gillet 1997). Their velocity is therefore close to zero, and they will begin to fall back onto the star. At the same time, the main shock is located in the upper atmosphere at approximately 1.35 times the photospheric radius. It always propagates outward, but at low velocity since it does no longer produce a blueshifted emission component within the Hα profile: the shock is no longer radiative.

In the meantime, the layers above the shock have not yet completed their infalling motion because of the sodium line doubling. Their average velocity is clearly supersonic since the red component is shifted by about 50 km s^{-1}.

The supersonic infalling motion of the highest atmospheric layers compresses the gas located in front of the shock more and more. The latter also contributes to the compression process by its opposite movement. Therefore, the third Hα emission is produced within the strongly compressed zone, hence high-temperature zone, that exists immediately above the shock front.

4.6. Compression zone

With the extraction technique used (a sum of Gaussians), the consecutive profile of the third emission appears rough.

In particular, the shape of the line profile does not seem accurate enough (reality of asymmetries, width variability, etc.) to derive a physical interpretation, especially in 2013. However, in particular through the EW and the RF, it is clear that the intensity of the emission increases after its appearance, reaches a maximum, and then decreases before finally disappearing (see Fig. 7).

This behavior is also expected to be observed for the FWHM, but this is not the case for the 2013 night. This night shows deeper telluric lines and a lower S/N than the 2014 night. Thus, for 2013, it is more difficult to extract the third emission.

The limit of the extraction method could also affect the V_{e3} measured radial velocities. Considering the 2013 night, the V_{e3} decreases from +36 km s^{-1} to +30 km s^{-1} ($\varphi \sim 0.20$ and 0.25), while for the 2014 night, the decrease is from +38 km s^{-1} to +29 km s^{-1} ($\varphi \in [0.3; 0.4]$). This general trend, a low, continuous decrease (starting from $\varphi \sim 0.2$ for the 2013 night) for both nights, is related to an increasing atmospheric compression. Therefore, the compression zone producing the emission is slowed down during its fall onto the star. Compared to the 2013 night, the V_{e3} value for the 2014 night is higher (+38 km s^{-1} at $\varphi = 0.33$). This would confirm that from one Blazhko cycle to another (which differ by about 10%), the amplitudes of the atmospheric dynamics can be very different.

This point seems to be well correlated with the observation of shock velocities that vary significantly from one cycle to another (Gillet et al., in prep.). Unfortunately, to confirm this point for these two nights of 2013 and 2014, we have no observations around phase 0.92 with which to determine an estimate of the shock velocity.

4.7. Comparison of the second and third apparitions

The second apparition consists of a small blueshifted emission, while the third apparition is a very weak redshifted emission. Both are interpreted as a consequence of the compression of the highest atmospheric layers on the deepest layers.

The small blueshifted emission (second apparition) was discovered by Gillet & Crowe (1988) near the pulsation phase $\varphi = 0.72$. This emission is visible during a relatively small phase interval ($\Delta\varphi \approx 0.1$). Its physical origin could be the result of a collision between the layers of the upper atmosphere with the photospheric layers during the infall phase of the ballistic motion. During this phase interval, all atmospheric layers contract and a luminosity bump occurs in the light curve (Gillet & Crowe 1988). The emission occurs just before the minimum radius at $\varphi \sim 0.92$, when the main shock emerges from the photosphere (Fokin & Gillet 1997). Because the gravity of RR Lyr is much higher ($g_\star \sim 250$ cm s^{-2}) than that of Classical Cepheids ($g_\star \sim 20-110$ cm s^{-2}), W Virginis stars ($g_\star \sim 15$ cm s^{-2}), or RV Tauri stars ($g_\star \sim 4$ cm s^{-2}), we must expect a high atmospheric compression rate at the end of the ballistic motion of the atmosphere.

Consequently, depending on the amplitude of the ballistic motion, that is, of the shock intensity of the preceding pulsation cycle, the compression rate may be sufficiently high to produce a strong heating of the gas, and a consecutive luminosity bump is observed. Because the infall velocity of the gas can become supersonic, especially at the end of the ballistic motion, a shock front moving outward in mass when the pulsation phase increases can be produced. This is the reason for the appearance of a blueshifted emission. The observation of RR Lyr presented in Gillet & Crowe (1988) shows that the emission is blueshifted by 79 km s^{-1}, which is indeed a supersonic speed. Finally, this emission is induced by the ballistic motion of atmospheric layers that is induced by, and thus its amplitude depends on, the main shock emerging in the photosphere at the beginning of the cycle. Therefore, the second emission is not directly produced by the main shock because it is not yet present in the atmosphere.

The very small redshifted emission (third apparition) occurs around the pulsation phase $\varphi = 0.30$ during an appreciable phase interval ($\Delta\varphi \sim 0.2$), twice as long as that of the second apparition. When the third emission appears near the phase $\varphi \sim 0.19$, the deepest photospheric layers propagate outward in the atmosphere while the highest layers have not completed their infalling motion (sodium line doubling). Consequently, the motion of low and high atmospheric layers originates in two different but consecutive pulsation cycles, introducing a coupling between these pulsation cycles. This coupling is absent when all atmospheric layers have enough time to complete their dynamical relaxation, as for low-amplitude pulsators.

Finally, the third apparition is the direct consequence of the high stellar gravity of RR Lyr. It generates a strong infall motion of the highest part of the atmosphere. This may explain why the third emission is not observed in other radially pulsating stars, except perhaps for long-period Cepheids, which have a stellar gravity ten times lower than that of RR Lyrae, and which is is interpreted as a P Cygni profile (Nardetto et al. 2008; Gillet 2014). This profile would be the consequence of the shock shell propagation in the high atmosphere.

The physical origin of the secondary and third emissions is thus not the same. The second emission is a consequence of the differential infall velocity between high and deep layers. The infall motion of the deepest photospheric layers is slowed down by the increasing compression on the high-density subphotospheric layers, while the highest layers continue their accelerated infall motion because of the low gas density in the high atmosphere. The third emission is the encounter between two layers of opposite motion: the lowest and highest parts of the atmosphere. This causes a compression zone that is located in front of the shock wave, which induces the observed redshifted emission. Thus, there are two different driving mechanisms: (i) the lowest layers are driven by the main shock, which rises in the atmosphere and reverses the movement of the layers falling onto the star; (ii) the layers are driven by gravity.

Finally, the two emissions are the result of a compression phenomenon caused by atmospheric dynamics. They are not simply a consequence of the passage of a rising shock wave within the atmosphere.

4.8. Influence of the Blazhko phase

In Fig. 8 we show the third apparition in the Hα line profile independent of the Blazhko phases. In first approximation, the third emission does not present a higher intensity at Blazhko maxima than at other Blazhko phases. This is not at all the case when the Hα blueshifted emission occurs when the main shock passes through the photosphere near $\varphi = 0.94$ (Chadid & Gillet 1997).

The third emission appears when the shock is located in the high atmosphere ($\varphi = 0.188-0.407$). In this phase interval, the shock is already far away from the photosphere ($1.35\,R_{ph}$), and as discussed above, the shock velocity becomes very weak. It is even probable that the shock loses its radiative nature, that is to say, it is no longer able to produce hydrogen emission. We recall that the third Hα emission component is produced by the atmospheric compression located in front of the shock.

Consequently, the intensity of the third Hα emission does not depend solely on the shock velocity of the previous pulsation

cycle, but more directly on the atmospheric dynamics. Thus, the impact of the Blazhko phase, that is, the shock amplitude, is significantly reduced at this distance from the star. The intensity of the third emission also depends on the intensity of the main shock of the current pulsation cycle since it is located between the ascending and descending atmospheric layers. The intensity of the third emission is a function of the intensities of the two main waves: that of the current cycle and that of the preceding cycle. It should be noted, however, that the influence of this latter shock is not as direct as the influence of the first shock, but only because of the ballistic motion of the atmosphere it has initiated.

Finally, the intensity of the third emission depends more or less directly on the intensity of the two main shock waves that belong to two consecutive pulsation cycles because their intensity is considerably reduced at high altitude. This may be the reason why the intensity dependence of the third Hα emission is not so obvious.

New observations with high S/N should enable us to quantify this marginal dependence of the Blazhko phase on the strength of the third emission.

5. Conclusion

We presented for the first time a set of observations of the Hα third emission in RR Lyr, the prototype of the RR Lyrae stars. This very weak emission appears as a hump within the red wing of the Hα line. It is observed around $\varphi \sim 0.30$ at a stellar rest frame velocity of about 30 km s^{-1}. This phenomenon lasts for about 20% of the pulsation period during pulsation phases $\varphi = 0.188-0.407$. The maximum intensity of this third emission with respect to the continuum is 13%.

For the night 2017-03-26 ($\varphi \sim 0.227$, $\psi = 0.44$), when the Hα third emission was present, the Na I lines double. This line doubling is intepreted as opposite motions between the upper atmosphere that is still falling back onto the star, and deeper layers dragged by the main outward shock wave. The high stellar gravity of RR Lyr plays a decisive role in the development of the shock by attenuating the amplitude of the ballistic motion of the atmosphere. The strong damping of the shock intensity prevents the production of any emission component within the Hα profile that would be formed in the shock wake. Thus, the shock is no longer radiative, and is probably close to its complete dissipation in the upper layers of the atmosphere.

Conversely, the free fall of the upper atmosphere is highly supersonic because the sodium red component is redshifted by 50 km s^{-1}. The Hα third emission would be due to the excitation of hydrogen atoms by the dynamical compression induced by the infalling motion of the atmosphere. From measuring the velocity of the redshifted emission, it appears that the compression region is supersonic as well.

It would be interesting to determine whether this compression process in the upper atmosphere also occurs in other RR Lyrae stars and even in other types of pulsating stars such as RV Tauri stars and classical Cepheids, since these stars also have high-intensity shocks and significant atmospheric extensions.

Finally, the data and work presented in this paper demonstrate further the increasing role of the amateur spectroscopy community in stellar surveys.

Acknowledgements. We thank Lux Stellarum and the French OHP-CNRS/PYTHEAS for their support. The present study has used the SIMBAD data base operated at the Centre de Données Astronomiques (Strasbourg, France) and the GEOS RR Lyr data base hosted by IRAP (OMP-UPS, Toulouse, France), created by J. F. Le Borgne. This research made use of SpcAudace, an open-source spectroscopic toolkit hosted at `http://spcaudace.free.fr` and written by B. Mauclaire (ARAS group, France). We also thank P. Valvin for his useful reading. We especially thank the referee for their very careful reading of the manuscript and pertinent remarks. And we gratefully acknowledge Astrid Peter for her very wise reading of the final version of this paper.

References

Baranne, A., Queloz, D., Mayor, M., et al. 1996, A&AS, 119, 373
Blažko, S. 1907, Astron. Nachr., 175, 325
Chadid, M., & Gillet, D. 1996, A&A, 308, 481
Chadid, M., & Gillet, D. 1997, A&A, 319, 154
Chadid, M., & Preston, G. W. 2013, MNRAS, 434, 552
Chadid, M., Kolenberg, K., Aerts, C., & Gillet, D. 1999, A&A, 352, 201
Fadeyev, Y. A., & Gillet, D. 2004, A&A, 420, 423
Fokin, A. B., & Gillet, D. 1997, A&A, 325, 1013
Fossati, L., Kolenberg, K., Shulyak, D. V., et al. 2014, MNRAS, 445, 4094
Gillet, D. 2014, A&A, 568, A72
Gillet, D., & Crowe, R. A. 1988, A&A, 199, 242
Gillet, D., & Fokin, A. B. 2014, A&A, 565, A73
Gillet, D., Burnage, R., Kohler, D., et al. 1994, A&AS, 108, 181
Gillet, D., Sefyani, F. L., Benhida, A., et al. 2016, A&A, 587, A134
Ginsburg, A., & Mirocha, J. 2011, PySpecKit: Python Spectroscopic Toolkit, Astrophysics Source Code Library [record ascl:1109.001]
Hill, S. J. 1972, ApJ, 178, 793
Hobbs, L. M. 1978, ApJ, 222, 491
Kovács, G. 2016, Coms. of the Konkoly Observatory Hungary, 105, 61
Le Borgne, J. F., Poretti, E., Klotz, A., et al. 2014, MNRAS, 441, 1435
Nardetto, N., Groh, J. H., Kraus, S., Millour, F., & Gillet, D. 2008, A&A, 489, 1263
Pickering, E. C., Colson, H. R., Fleming, W., et al. 1901, ApJ, 13, 226
Preston, G. W. 2011, AJ, 141, 6
Preston, G. W., Smak, J., & Paczynski, B. 1965, ApJS, 12, 99
Savitzky, A., & Golay, M. J. E. 1964, Anal. Chem., 36, 1627
Schwarzschild, M. 1952, Transactions of the IAU VIII (Roma, Oosterhoff, P. Th.: CUP), 8, 811
Smolec, R. 2016, in 2016, 37th Meeting of the Polish Astronomical Society, eds. A. Różańska, & M. Bejger, 3, 22
Struve, O., & Blaauw, A. 1948, ApJ, 108, 60
Thizy, O., & Cochard, F. 2011, in Active OB Stars: Structure, Evolution, Mass Loss, and Critical Limits, eds. C. Neiner, G. Wade, G. Meynet, & G. Peters, IAU Symp., 272, 282
Wagenblast, R., Bertout, C., & Bastian, U. 1983, A&A, 120, 6
Xiong, D. R., Cheng, Q. L., & Deng, L. 1998, ApJ, 500, 449